Biomedical Signal Processing and Control 86 (2023) 105240

Contents lists available at ScienceDirect

Biomedical Signal Processing and Control

journal homepage: www.elsevier.com/locate/bspc

Modeling peripheral arterial and venous pressure signals with integral pulse frequency modulation

Md Abul Hayat [a], Jingxian Wu [a,*], Sam Stephens [b], Hanna K. Jensen [c], Adrià A. Villafranca [c], Joseph A. Sanford [c], Kevin W. Sexton [c], Morten O. Jensen [b]

[a] Department of Electrical Engineering, University of Arkansas, AR 72701, USA
[b] Department of Biomedical Engineering, University of Arkansas, AR 72701, USA
[c] Department of Surgery, University of Arkansas for Medical Sciences, AR 72205, USA

ARTICLE INFO

Keywords:
Peripheral blood pressure signals
Peripheral arterial pressure
Peripheral venous pressure
Integral pulse frequency modulation
Respiratory rate estimation
Heart rate variability

ABSTRACT

This paper proposes a novel mathematical modeling framework for peripheral arterial and peripheral venous blood pressure signals from porcine experiments. Peripheral blood pressure signals can be acquired using regular catheters during standard patient treatment. The minimally invasive nature and ubiquitous availability of catheters render it an ideal candidate for various applications. However, there is no analytical model for peripheral blood pressure signals in the literature. We address this issue by proposing a model for these signals under the integral pulse frequency modulation (IPFM) framework. The model incorporates the impacts of physiological phenomena, such as the heartbeat pulse shape variation, heart rate variability, respiratory rate, etc. The model parameters are obtained by applying the IPFM model to experimental data collected from four pigs under different anesthetic dosages. The proposed model can fit the experimental data with Pearson correlation coefficients greater than 0.99 and 0.90 for arterial and venous blood pressure signals, respectively. The performance of model-synthesized data on the classification of two different anesthesia is comparable with experimental data. Parameters like pulse shape and duration can also work as distinguishable features under different anesthesia. We also proposed a way to distinguish respiratory-induced heart rate variability from other causes. Increasing doses of vasodilating anesthesia is similar to going from dehydration to hydration. Thus the results obtained in this study can be extended in distinguishing hydrated and dehydrated subjects. This model can be extended to similar biomedical signals like photoplethysmography, cerebral blood flow velocity, and Doppler waveforms.

1. Introduction

Peripheral arterial pressure (PAP) and peripheral venous pressure (PVP) signal properties can provide valuable information regarding the clinical conditions of patients. For example, the PVP signal is strongly correlated with the central venous pressure (CVP) signal [1,2]. CVP is the pressure in the first and second-order branches of veins that drain into the right atrium of the heart. However, the collection of CVP relies on the invasive placement of a central monitor and contains significant risk and time to place correctly. PAP or PVP signals, on the other hand, can be collected with regular intravenous and intra-arterial catheters that are widely available and routinely used. The minimally invasive nature combined with the ubiquitous availability of catheters renders it as an ideal candidate for a wide range of applications in patient care. For example, PVP signals have been used in a wide range of medical scenarios, such as pediatric surgery [3], laparoscopic colorectal surgery [1], craniotomy or complex spine surgery [4], patients with acute decompensated heart failure [5], etc.

The study and analysis of PVP signals have attracted considerable attention recently [6–12]. It is shown that PVP signals can be used to predict dehydration in the pediatric population [13]. PVP signals are used to assess the dehydration level of infants suffering from pyloric stenosis and hemorrhage during craniosynostosis repair [14]. PVP signals are also related to other peripheral blood pressure signals. A recent study shows that the PVP signal is strongly correlated with peripheral arterial pressure (PAP) [15] signal. The Photoplethysmogram (PPG) signal is similar in nature to PVP signal in that both are directly related

* Corresponding author.
E-mail addresses: mahayat@uark.edu (M.A. Hayat), wuj@uark.edu (J. Wu), sxs094@uark.edu (S. Stephens), hkjensen@uark.edu (H.K. Jensen), aaabellavillafranca@uams.edu (A.A. Villafranca), jasanford@uams.edu (J.A. Sanford), kevin.sexton@uams.edu (K.W. Sexton), mojensen@uark.edu (M.O. Jensen).

https://doi.org/10.1016/j.bspc.2023.105240
Received 21 March 2023; Received in revised form 26 June 2023; Accepted 3 July 2023
Available online 15 July 2023
1746-8094/© 2023 Published by Elsevier Ltd.

to blood flow, and the relationship between PPG and PVP signals is studied in [16]. However, there is a lack of research on the modeling of PAP and PVP signals. Parametric modeling of these signals can help us understand the generation process behind the signals, thus providing insights into their relations to various physiological phenomena.

Signal modeling is an important tool that can be used to understand the physiology and generative process behind a biomedical signals. It also helps to quantify and predict the changes in the signal under different internal and external impact circumstances. This can significantly improve treatment outcomes in many situations, which is the overall goal of this work. Several models are developed to represent the behaviors of PPG signals. For example, in [17], the PPG signal is modeled by using a synthesis-by-analysis technique. Synthetic PPG models are developed to generate PPG waveforms with two combined Gaussian functions, and they can model both regular and irregular heartbeats [18,19]. A modulation-based PPG model is proposed in [20] to extract vital signs from PPG signals. There are a wide range of models for ECG signals. In [21], a modified Zeeman model with an artificial neural network is developed to generate ECG signals. In [22], 12-lead ECG signals are modeled by using bidomain equations coupled to a phenomenological ionic model in the heart and a generalized Laplace equation in the torso. An ECG model that simulates the main pacemakers in the heart by using a set of three nonlinear oscillators produced by discretized reaction-diffusion system is proposed in [23]. In [24], Gaussian functions along with hybrid optimization methods have been proposed to model ECG morphology in different cardiac dysrhythmias. To the best of our knowledge, no analytical model is available for peripheral blood pressure signals.

In this paper, we propose to build an analytical model for PAP and PVP signals with the framework of integral pulse frequency modulation (IPFM). IPFM was first introduced in [25] for analyzing nervous systems. It was later applied to model heart rate variability (HRV) studies [26,27]. IPFM uses irregularly spaced spikes to imitate the physical properties behind HRV [28]. Improved HRV modeling and analysis with IPFM are presented in [29–31]. In all existing works, the IPFM model has only been used to model the onset of pulses, and none can be found to model the signal itself. To the best of our knowledge, the IPFM model was never applied to PAP and PVP signals before.

In recognition that the peripheral blood pressure signals are affected by HRV through frequency modulation (FM) and respiration signals through amplitude modulation (AM), we propose to capture these physiological phenomena by using IPFM. The utilization of IPFM allows us to focus on the physiology of peripheral blood pressure signals without dealing with complex spectrum analyses of AM-FM signals. Unlike existing IPFM models that focus solely on the onset of pulses, the proposed work combines IPFM with convolution analysis, which allows us to model the shape of the peripheral waveforms.

Under the IPFM framework, the proposed model is developed by analyzing the properties of PAP and PVP signals collected from pig experiments. The newly proposed model is more general than the modulation model in [20]. The model parameters are learned by fitting the developed IPFM model to the experimental data. The accuracy and efficacy of the model are evaluated by comparing model-synthesized data with experimental data. It is demonstrated that the proposed model matches very well with the experimental results.

The rest of the paper is organized as follows. Section 2 discusses the experimental setup and data acquisition process. The proposed IPFM modeling framework is introduced in Section 3. In Section 4, a numerical modeling fitting method is proposed to estimate the model parameters by fitting the model to the experimental data. The performance of the model is evaluated in Section 5. Section 6 discusses some qualitative properties of some of the model parameters, and Section 7 concludes the paper.

Table 1
Pig subjects used in this study.

Subject	Weight (kg)	Age (weeks)	Controlled blood loss (ml)	Blood-weight ratio (ml/kg)
Pig1	70	16	1270	18.14
Pig2	74	17	923	12.47
Pig3	74	17	963	13.01
Pig4	73	17	910	12.47

2. Experiment setup and data acquisition

This section describes the setup of the experiment, the demographics of the animal subjects, the data acquisition system, and the data collection workflow at different stages of anesthesia, and the overall design of the experiment.

2.1. Pig demographics

In this study, four female pigs were used. All pigs were between ages 16–17 weeks, at a weight of 70–74 kg at the time of the experiment. The detailed demographics are listed in Table 1. During the experiment, the pigs were anesthetized and experienced controlled blood loss. The average blood-weight ratio is 13.97 ml/kg. The study was performed following the approval of the University of Arkansas for Medical Sciences (UAMS) institutional animal care and use committee.

2.2. Data acquisition system

Millar Mikro-Tip® solid-state catheters with a pressure sensor(s) provide high-fidelity cardiovascular pressures (the heart and vascular system) at the source in small animals [32]. Two Millar pressure catheters are used at the brachial artery and brachial vein to collect arterial (PAP) and venous (PVP) pressure signals, respectively. Fig. 1 is the schematic diagram of the data acquisition system. For Pigs 1 and 2, Millar catheters of size 5F (Millar SPR-350S) were used. Whereas, Millar catheters of size 2F (Millar SPR-320) were used for Pigs 3 and 4. Here, F indicates the French catheter scale (1F corresponds to an external diameter of 1/3 mm). Catheters were then connected to a pressure control unit (Millar PCU-2000) via catheter interface cables (ADInstruments PEC-10D). The output of the pressure control unit is then connected to a National Instruments (NI) USB-6009 data acquisition system.

While inserting the Millar catheters, the distance between the catheters was observed using ultrasound systems (BK500, BK Medical) to make sure they were within 3–4 cm apart. Datex Ohmeda Aestiva 5 (GE Healthcare) anesthesia machine was used to maintain mechanical ventilation greater than the respiratory rate of 0.2 Hz (12 bpm). At lower anesthetic levels a deviation from 0.2 Hz is expected. On the other hand, at higher anesthetic levels the pigs do not show self-breathing tendency, and the respiratory rate shows very little deviation.

It should be noted that this paper models the voltage signal recorded at the USB-6009 data acquisition system. The voltage (Volt) and the pressure (mmHg) are proportional to each other and are related in a linear relationship. Thus, the signal used in this study can have negative values.

2.3. Data collection workflow

After inserting and attaching the transducers, the pigs were anesthetized using Isoflurane ($C_3H_2ClF_5O$). Isoflurane, a widely used general anesthetic, and vasodilator is given via inhalation. Vasodilation and vasoconstriction are the widening and narrowing of blood vessels respectively. The amount of Isoflurane was changed to 1.8%, 2.5%,

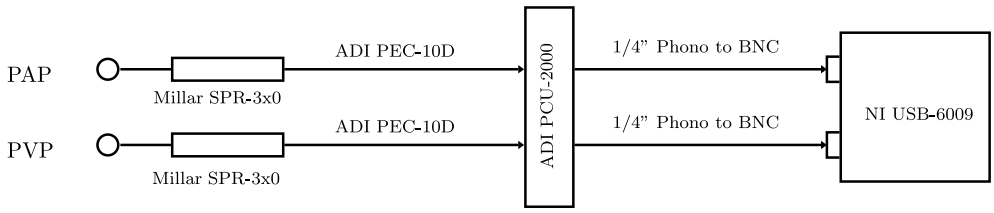

Fig. 1. Schematic diagram of peripheral arterial pressure (PAP) and peripheral venous pressure (PVP) signals being collected using Millar SPR-3x0 (solid-state) catheters with National Instrument USB-6009 data acquisition system.

Table 2
Data collection workflow.

Action	Amount	Abbreviation
Isoflurane (%)	[a]1.80	MAC-1
	[a]2.50	MAC-2
	[a]2.80	MAC-3
	2.00	
	1.50	
Propofol (mg/kg/min)	[a]0.10	PRO-1
	[a]0.15	PRO-2
	[a]0.20	PRO-3
	0.05	
Bleeding		
Propofol	0.05	
Isoflurane	1.50	
	2.00	

[a]Denote the data used in this paper.

2.8%, 2.0%, and 1.5% over time. In terms of minimum alveolar concentration (MAC), Isoflurane 1.8%, 2.5%, and 2.8% are considered MAC-1, MAC-2, and MAC-3, respectively.

Propofol ($C_{12}H_{18}O$), another widely used anesthetic and vasodilator, was injected into the veins following Isoflurane delivery. The amount of Isoflurane was changed to 0.10 mg/kg/min, 0.15 mg/kg/min, 0.20 mg/kg/min, and 0.05 mg/kg/min. At this stage, all pigs went through bleeding from the femoral artery of the right leg. The amount of blood loss for each pig is listed in Table 1. After bleeding, Propofol 0.05 mg/kg/min is followed by Isoflurane 1.5% and 2.00%.

Propofol 0.10 mg/kg/min, 0.15 mg/kg/min, and 0.20 mg/kg/min are denoted as PRO-1, PRO-2, and PRO-3, respectively in this paper. Also note that PRO-1 stage does not immediately start after MAC-3. The data collection workflow is summarized in Table 2.

In the original setup of this experiment, multiple other signals were collected. Based on the signal quality during the data collection procedure, this paper only deals with PAP and PVP signals. PAP and PVP signal acquisition processes do not show a blood clotting tendency in the Millar catheter. It should be made clear that this paper treats PAP and PVP signals as peripheral blood pressure signals as both are collected from the brachial artery and brachial vein respectively.

During dehydration or blood loss, humans and animals have the tendency to constrict blood vessels, i.e., narrowing of blood vessels that is also known as vasoconstriction. Vasodilators such as Isoflurane and Propofol can on the other hand widen the blood vessels. So, during the MAC-3 stage the blood vessels are wider compared to MAC-1. Thus compared to MAC-3, MAC-1 has a similar effects as the dehydrated state. The same reasoning holds for the PRO stages. This motivates the study of the various peripheral blood pressure signals under different stages of anesthesia in this experiment.

3. Parametric signal modeling

The two main components embedded in peripheral blood pressure signals are heart rate (with harmonics) and respiratory rate signals. These two signals are modulated with each other.

However, the heart rate does not remain constant over time. There is always a time-dependent variation in heart rate. The variation in heart rate is called heart rate variability (HRV). HRV is an important indicator of the autonomic nervous system (ANS). ANS is a network of nerves that handles unconscious tasks like heartbeat and breathing. This is why the HRV is an important physiological and neurological indicator of sympathetic (quick "fight-or-flight" response) and parasympathetic (slow response) activities of ANS. High HRV indicates a healthy nervous system that is responsive to both sympathetic and parasympathetic inputs. This is why HRV is still a highly active field of research.

HRV can be contributed by multiple sources. The main cause of HRV is respiration. Heart rate increases and decreases with inhalation and exhalation, respectively. Such respiratory-induced HRV is called respiratory sinus arrhythmia (RSA). There are also other long-term sources of HRV such as ANS imbalance, heart diseases (like Arrhythmia), stress, poor sleep, unhealthy diet, lack of exercise, etc. The signal model proposed in the paper isolates the impact of respiration from heart rate signal.

The IPFM-based parametric model is developed based on the hypothesis that the occurrences of pulse onsets are initiated by a continuous-time modulating signal $m(t)$, which has certain physiological interpretations [28,33]. A pulse onset trigger impulse is generated when the integration of $m(t)$ reaches a certain threshold. It is assumed that $|m(t)| \ll 1$ and its Fourier transform $\mathcal{F}\{m(t)\} = M(\omega)$ is bandlimited with negligible power spectral density beyond a frequency typically around 0.4–0.5 Hz [28,33]. It is also assumed that $m(t)$ is a zero-mean signal, i.e., $M(0) = 0$.

Denote t_k as the time instant of the onset or occurrence of the kth heartbeat. Without loss of generality, it is assumed that the first pulse onset occurs at time $t_0 = 0$ and $m(t)$ is causal [34], that is, $m(t) = 0$ for $t < 0$. Based on the principle of the IPFM model [28], the following equation relates t_k with $m(t)$ [28, Equation (1)]

$$T = \int_{t_k}^{t_{k+1}} [1 + m(t)]dt, \tag{1}$$

or alternatively

$$k = \int_0^{t_k} \frac{1 + m(t)}{T} dt, \tag{2}$$

where T is the mean heart rate interval in seconds, and $\frac{1}{T}$ is the mean heart rate in Hertz.

In the IPFM model, the continuous-time signal $m(t)$ models the dynamic variability of the heart rate. When $m(t) = 0$, there will be no HRV with $t_{k+1} - t_k = T$ for all $k \in \mathbb{Z}^+ = \{0, 1, 2, \ldots\}$.

Another related and important signal is the heart timing signal $\theta(t_k)$, which is defined as the deviation of heartbeat occurrence time t_k from the mean occurrence time kT [28]. From (2), we have

$$\theta(t_k) = kT - t_k = \int_0^{t_k} m(\tau)d\tau. \tag{3}$$

Eq. (3) presents a non-uniformly sampled version of $\theta(t)$. The continuous-time heart timing signal $\theta(t)$ can be approximated by performing spline interpolation over the discrete time samples, $\theta(t_k)$, for $k \in \mathbb{Z}^+$. In this paper, cubic spline interpolation is used to estimate $\theta(t)$

from $\theta(t_k)$. The knowledge of $\theta(t)$ can be used to estimate the signal $m(t)$ as

$$m(t) = \frac{d\theta(t)}{dt}. \tag{4}$$

The conventional IPFM framework can only be used to model the onset of pulses, and it cannot be readily applied to model continuous-time waveforms such as the PAP or PVP signals. In this paper, we extend the IPFM model to model the continuous-time waveform of the signal, instead of just modeling the onset pulses as in the literature. Based on this proposed model, the respiratory signal, $r(t)$, is modulated with the heart rate signal, $x(t)$. The signal $x(t)$ is not just the heart rate and its higher-order harmonics. However, we refer to it as the heart rate signal for simplicity. Both $r(t)$ and $x(t)$ are constituent components of PAP or PVP signals. Based on this idea, the continuous-time waveform $x(t)$ can be modeled by performing convolution between the IPFM pulses with the single heartbeat pulse of the heartbeat signal.

A single heartbeat pulse is defined as $p(t)$ with support T. Under the proposed model, the heart rate signal in the time domain can be represented as

$$x(t) = \sum_k p\left(\frac{T}{t_{k+1} - t_k} t\right) \otimes \delta(t - t_k), \tag{5}$$

where $\otimes$ denotes continuous time convolution. Given that $|m(t)| \ll 1$, we employ the approximation that $t_{i+1} - t_i \approx T$, and (5) can be simplified to

$$x(t) = p(t) \otimes \sum_k \delta(t - t_k). \tag{6}$$

This approximation is only used to facilitate the modeling process to demonstrate how different components of the signal are interacting with each other, and the final modeled signal still follows (5).

Once the pulse onset time instants $\{t_k\}_{k\in\mathbb{Z}^+}$ are known, a non-uniformly spaced pulse train is defined as

$$s(t) \triangleq \sum_k \delta(t - t_k), \tag{7}$$

$$= \frac{1 + m(t)}{T} \left[1 + 2\sum_{n=1}^{\infty} \cos\left(\frac{2n\pi}{T}\left(t + \theta(t)\right)\right)\right]. \tag{8}$$

Detailed derivations of (8) is in Appendix A. The second equality follows from the fact that $|1 + m(t)| = 1 + m(t)$ as $|m(t)| \ll 1$. As a sanity check, when $\theta(t)$ is constant, i.e., $m(t) = 0$, then $s(t)$ corresponds to an impulse train.

Using the definitions above, the observed PAP or PVP signal $y(t)$ can then be modeled as

$$y(t) = \tau(t) + \left[\alpha + r(t)\right]\left[\beta + x(t)\right] \tag{9}$$

where $\tau(t)$ is a slow-changing bias or drift introduced by the data acquisition system, $r(t)$ is the respiratory signal, $x(t) = p(t) \otimes s(t)$ is the heart rate signal, and α and β are the DC offsets of $r(t)$ and $x(t)$, respectively. The signal $\tau(t)$ has zero mean, hence the DC value of the signal $y(t)$ is $\alpha\beta$.

Eq. (9) incorporates the fact that $x(t)$ is amplitude modulated by $r(t)$. From (8), it is clear that the signal $s(t)$ and thus heart rate signal $x(t)$ are dependent on $m(t)$. The signal $x(t)$ does not contain any component of $r(t)$. This property separates the impact of the respiratory signal $r(t)$ from the modulating signal $m(t)$ and the heart rate signal $x(t)$. Based on the physiological conditions, the signals $m(t)$ and $r(t)$ can be correlated. In that case, the strength of the correlation between $m(t)$ and $r(t)$ can indicate the strength of RSA on HRV. The parametric model presented in (9) includes the effects of heartbeat, respiration, HRV, and their mutual interactions. The parameters of the model can be estimated or learned by fitting the model to the experimental data.

4. Model fitting

In this section, both numerical and computational approaches are employed to model the experimental data collected from the pig subjects by using the theoretical foundations of the previous section.

4.1. Model reformulation

Given that the measured signals contain impacts from multiple physiological factors at different frequency ranges, we reformulate the signal model to reflect the diverse signal compositions. The reformulation will facilitate the model fitting process.

From (8), define the heart rate and its harmonics as

$$h(t) \triangleq 2\sum_{n=1}^{\infty} \cos\left(\frac{2n\pi}{T}\left(t + \theta(t)\right)\right). \tag{10}$$

The pulse train $s(t)$ defined in (8) can then be alternatively represented as

$$s(t) = \left[\frac{1 + m(t)}{T}\right][1 + h(t)],$$
$$= \frac{1}{T} + \frac{1}{T}m(t) + \frac{1}{T}h(t) + \frac{1}{T}m(t)h(t). \tag{11}$$

Combining the definition of $s(t)$ from (7) with (6) gives

$$x(t) = p(t) \otimes s(t) = \gamma + \frac{1}{T}p(t) \otimes h(t) + q(t), \tag{12}$$

where

$$\gamma \triangleq \frac{1}{T}\int_0^T p(t)dt, \tag{13}$$

$$q(t) \triangleq \frac{1}{T}p(t) \otimes [m(t)(1 + h(t))]. \tag{14}$$

Combining (9) and (12) yields,

$$y(t) = \tau(t) + \alpha\beta + \beta r(t) + \alpha x(t) + x(t)r(t),$$
$$= \tau(t) + y_{\text{LF}}(t) + y_{\text{HF}}(t), \tag{15}$$

where

$$y_{\text{LF}}(t) \triangleq \alpha(\beta + \gamma) + (\beta + \gamma)r(t),$$
$$= \left[\beta + \gamma\right]\left[\alpha + r(t)\right], \tag{16}$$

$$y_{\text{HF}}(t) \triangleq [\alpha + r(t)]\left[\frac{1}{T}p(t) \otimes h(t) + q(t)\right],$$
$$= [\alpha + r(t)]\tilde{x}(t). \tag{17}$$

Here, $\tilde{x}(t) \triangleq x(t) - \gamma = \frac{1}{T}p(t) \otimes h(t) + q(t)$.

In the reformulated model given in (15), the pressure signal $y(t)$ is decomposed into three components, the very slow changing bias $\tau(t)$, the low-frequency component due to respiratory activities $y_{\text{LF}}(t)$, and the high-frequency component $y_{\text{HF}}(t)$ dominated by heart rate. Also, it should be noted that γ is the DC value of the signal $x(t)$ and thus $\tilde{x}(t)$ is a zero-mean signal.

4.2. Model fitting

With the reformulated model presented in (15), we can numerically estimate the reformulated model parameters from the experimental data $y_r(t)$. Details of the model fitting process are given in Algorithm 1.

The model fitting process is developed by separating the bias $\tau(t)$, the low-frequency component $y_{\text{LF}}(t)$, and the high-frequency component $y_{\text{HF}}(t)$, from the experimental data.

At first, the recorded experimental data $y_r(t)$ is bandlimited by passing through a low pass filter with cutoff frequency $f_c = 15$ Hz to remove noises from the data collection process. The stopband attenuation of the low pass filter is 60 dB. The cutoff frequency is chosen based on the fact that the fundamental frequency of heart rate is usually at 2 Hz or lower, thus its harmonics are usually well below 15 Hz. Denote the output of the low pass filter as $y(t)$.

The bias $\tau(t)$ is a small drift introduced by the data acquisition system, and it changes much slower than the respiratory or heart rate signals. The bias signal is estimated using a simple moving average (low pass) filter of a window length of 30 s. Fig. 2 shows an example of the experimental data, $y_r(t)$, the corresponding bandlimited signal, $y(t)$, and

the slow changing bias, $\tau(t)$, from the PAP signal collected from Pig-2 during MAC-2.

The bias-corrected signal, $\tilde{y}(t) \triangleq y(t) - \tau(t)$, passes through a low pass filter with cutoff frequency f_0 to separate the low and high-frequency components, $y_{\text{LF}}(t)$ and $y_{\text{HF}}(t)$, respectively. The cutoff frequency f_0 is chosen below the heart rate but above the respiratory harmonics. In this paper, we use $f_0 = 0.5$ Hz, and the stopband attenuation of this low pass filter is 60 dB. Examples of $\tilde{y}(t)$ with the corresponding $y_{\text{LF}}(t)$ and $y_{\text{HF}}(t)$ from Pig-2 during MAC-2 are shown in Fig. 3.

The model parameters, α, $\beta+\gamma$, $r(t)$, and $\tilde{x}(t)$ can then be estimated by using the filtered signals, $y_{\text{LF}}(t)$ and $y_{\text{HF}}(t)$. From (17), the high-frequency component $y_{\text{HF}}(t)$ can be equivalently considered as $\tilde{x}(t)$ amplitude modulated by the low-frequency signal $\alpha+r(t)$. Thus the low-frequency modulating signal, $\alpha + r(t)$, is embedded in the amplitude of $y_{\text{HF}}(t)$. Consequently, $\alpha + r(t)$ can be estimated by performing envelope detection over $y_{\text{HF}}(t)$ as shown in Fig. 4. Denote the upper and lower envelopes of $y_{\text{HF}}(t)$ as $e_u(t)$ and $e_l(t)$, respectively. Under the assumption of ideal envelope detection, we have $e_u(t) = -e_l(t) = \alpha + r(t)$. Then the DC offset α can be estimated as

$$\alpha = \frac{\bar{e}_u - \bar{e}_l}{2}, \tag{18}$$

where $\bar{e}$ denotes the time average of the signal $e(t)$ and $r(t)$ is assumed to be a zero-mean signal. Envelopes are estimated using spline interpolation over local maxima using the "envelope(_, _, 'peak')" function of Matlab. As can be seen from (16), the mean value of the y_{LF} signal is $\bar{y}_{\text{LF}} = \alpha(\beta+\gamma)$. Similarly, the parameter $\beta+\gamma$ can be estimated as

$$\beta + \gamma = \frac{\bar{y}_{\text{LF}}}{\alpha}. \tag{19}$$

Given the parameters α and $\beta+\gamma$, the signals $r(t)$ and $\tilde{x}(t)$ can then be estimated by using (16) and (17) as

$$r(t) = \frac{y_{\text{LF}}(t)}{\beta+\gamma} - \alpha, \tag{20}$$

$$\tilde{x}(t) = \frac{y_{\text{HF}}(t)}{\alpha + r(t)}. \tag{21}$$

The signal $\tilde{x}(t)$ is the heart rate signal without the DC offset γ. A peak detection algorithm is applied to $\tilde{x}(t)$ to identify the time of systolic cycle onset or the beginning of a pulse as shown in Fig. 4. Details of the onset detection algorithm are given in Section 4.3. It should be noted that the onset detection algorithm is not applied on $y_{\text{HF}}(t)$ because, based on (17), it is modulated by $\alpha + r(t)$. To ignore the effect of $r(t)$, the onset detection is performed over $\tilde{x}(t)$ instead of $y_{\text{HF}}(t)$. This can be also observed in Fig. 4.

The onset detection algorithm is used to estimate the systolic cycle onset or the pulse onset time $\{t_k\}_{k\in\mathbb{Z}^+}$, which is then used to construct an estimate of the impulse train $s(t)$ defined in (7). After estimating $\{t_k\}_{k\in\mathbb{Z}^+}$, the mean pulse shape $\tilde{p}(t)$ is estimated by taking average from aggregating all the pulses. Ideally, the initial value $p(0)$ and the final value $p(T)$ of the pulse $p(t)$ should be equal. To make this happen, a linear normalization is performed on the mean pulse shape $\tilde{p}(t)$ as

$$p(t) = \tilde{p}(t) - \frac{\tilde{p}(T) - \tilde{p}(0)}{T} t.$$

Fig. 8 is an example of the estimated $p(t)$. Based on (13), the parameter γ can be easily estimated by taking the time average of the pulse $p(t)$. With the estimated parameters $\{t_k\}_{k\in\mathbb{Z}^+}$, T and $p(t)$, we can construct a synthesized model signal $\hat{x}(t)$ by using (5) (Step 7 in Algorithm 1). Once $\hat{x}(t)$ is constructed, we can construct a synthesized version of the overall signal by following Step 8 in Algorithm 1.

It should be noted that at Step 5 of Algorithm 1, the signal $\alpha + r(t)$ must be non-zero at all times to avoid dividing by zero. To make sure that this signal does not cross zero, a DC offset is added to the signal $y(t)$, when needed, without loss of generality. In the case of the PVP signal, an offset of 1 has been added to $y(t)$.

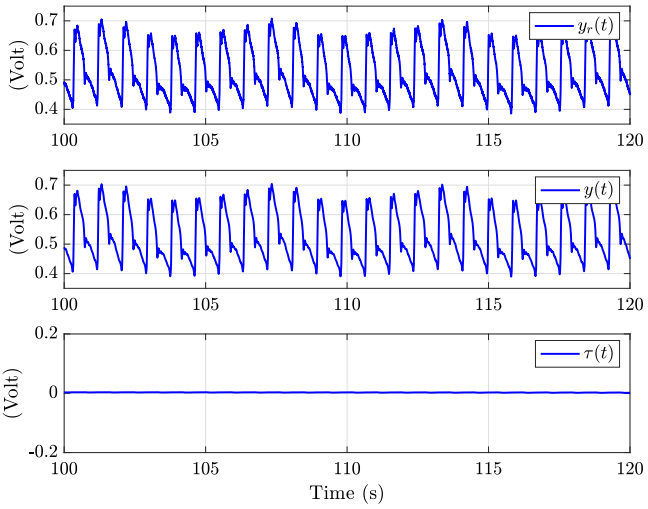

Fig. 2. Example of separating high-frequency noise and trend from recorded signal $y_r(t)$ (Pig-2 MAC-2 PAP). Here, $y(t)$ obtained after filtering $y_r(t)$ and $\tau(t)$ is zero-mean trend of the signal $y(t)$. Regarding $\tau(t)$, the whole signal recording has a mean zero.

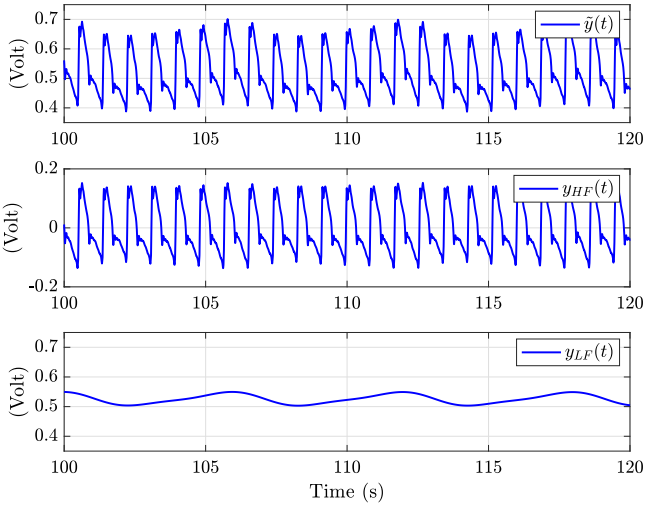

Fig. 3. Separating high-frequency component $y_{\text{HF}}(t)$ and low-frequency component $y_{\text{LF}}(t)$ from $\tilde{y}(t) = y(t) - \tau(t)$ signal (Pig-2 MAC-2 PAP). $y_{\text{LF}}(t)$ is a linear transformation of respiratory signal $r(t)$.

4.3. Pulse onset detection

Pulse onset detection is a crucial part of the signal modeling process. Based on the nature of the signal, two different kinds of onset detection algorithms are used.

For the PVP signals, the onset detection can be performed by using peak detection algorithms that are similar to the ones used for ECG [35], PPG [36] and other related signals [37]. In this paper, the onset is detected using "findpeaks()" function of Matlab on $-\tilde{x}(t)$. After detecting a peak, a certain time (in the range between 500–800 ms) is waited to find the next peak. The wait time depends on the fundamental heart rate frequency of the signal.

For the PAP signal, the onset detection is performed by using a surrogate signal defined as the Slope sum function (SSF) [38]. This SSF is basically the accumulation of non-zero slopes looking back in time over a certain duration (120 ms in this paper). The SSF signal has a sharp rise after the systolic onset. A threshold is selected (non-adaptive in this case as it is applied on $\tilde{x}(t)$ signal) by taking the average of the first 8 s of the SSF signal. If a point exceeds the threshold, a search is

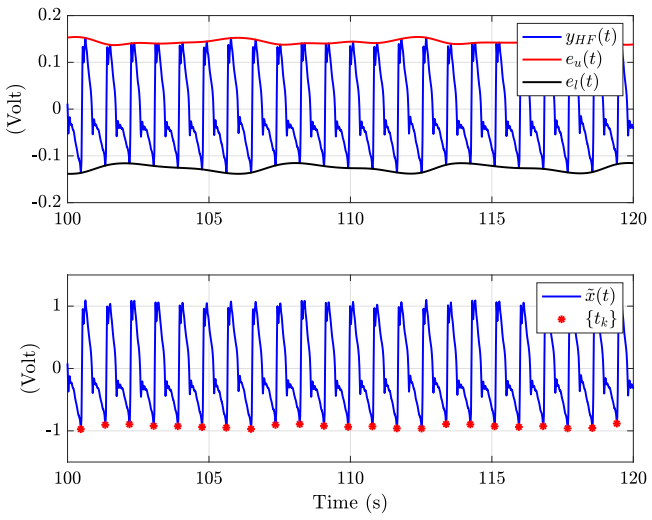

Fig. 4. Estimating envelope $e_u(t)$ and $e_l(t)$ from $y_{HF}(t)$ signal (Pig-2 MAC-2 PAP). The model aims to flatten the envelope for $\tilde{x}(t)$ signal.

Table 3
PAP and PVP Signal duration (unit: minutes).

Subject	MAC-1	MAC-2	MAC-3	PRO-1	PRO-2	PRO-3
Pig-1	21.08	13.79	2.42	20.58	16.94	9.89
Pig-2	18.74	6.45	22.30	20.01	12.50	13.31
Pig-3	20.84	20.37	19.89	33.43	19.43	30.38
Pig-4	20.12	19.97	10.00	20.39	21.34	20.39

performed on the neighborhood (60 ms before and after the crossing) to detect the onset. Once an onset is found, the process of searching for a new onset is paused for the next 500 ms. This method works well for PAP signals because it has a sharp change at systolic onset and the location and shape of the dicrotic notch do not cause trouble in the pulse onset detection procedure.

It should be also made clear that these algorithms are not always 100% correct in detecting onset time. There is false detection of onset time and the synthesized signal quality is compromised at those time instances.

5. Performance evaluation

In this section, the proposed model is applied to experimental PAP and PVP signals. The performance of the new model is evaluated by comparing the model-synthesized signals with their respective experimental counterparts in terms of both signal fidelity and their capabilities in classifying the different anesthetic stages of the animal subjects.

5.1. Dataset description

The duration of PAP and PVP signals under different MAC and PRO levels used in this paper are shown in Table 3. At each stage, the PAP and PVP signals are of the same duration and are synchronized. The sampling rate of all the signals is 1000 samples/s.

5.2. Model fitting performance

To evaluate the similarity between the experimental and model-synthesized signals, Pearson's correlation coefficient has been used. It has been used in similar papers [39,40] and defined as

$$\rho = \frac{\sum_i (y[i]-\bar{y})(\hat{y}[i]-\bar{\hat{y}})}{\sqrt{\sum_i (y[i]-\bar{y})^2}\sqrt{\sum_i (\hat{y}[i]-\bar{\hat{y}})^2}}. \tag{22}$$

Algorithm 1 IPFM model fitting of blood pressure signal

Input: Experimental signal $y_r(t)$
Output: Synthesized signal, $\hat{y}(t)$

1: Band-limiting the input signal $y_r(t)$ to discard frequency components beyond 15 Hz and this filtered signal is denoted as $y(t)$.
2: Apply a simple moving average filter with a window length of 30 s to extract the zero-mean bias $\tau(t)$ of the signal.
3: Apply a low-pass filter with cutoff frequency $f_0 = 0.5$ Hz to the bias-corrected signal, $\tilde{y}(t) = y(t) - \tau(t)$, to separate low and high frequency component $y_{LF}(t)$ and $y_{HF}(t)$ respectively as

$$\tilde{y}(t) = y(t) - \hat{\tau}(t) = y_{LF}(t) + y_{HF}(t).$$

4: Find the upper envelope $e_u(t)$ and lower envelope $e_l(t)$ of the signal $y_{HF}(t)$.
5: Estimate α, $\beta+\gamma$, $r(t)$ and $\tilde{x}(t)$ using the following equations

$$\alpha = \frac{\bar{e}_u - \bar{e}_l}{2},$$
$$\beta+\gamma = \frac{\bar{y}_{LF}}{\alpha},$$
$$r(t) = \frac{y_{LF}(t)}{\beta+\gamma} - \alpha,$$
$$\tilde{x}(t) = \frac{y_{HF}(t)}{\alpha + r(t)}.$$

6: The signal $\tilde{x}(t)$ is used to estimate $\{t_k\}_{k\in\mathbb{Z}^+}$ or $s(t)$, $p(t)$ and T using onset detection algorithm in 4.3. Pulse $p(t)$ is used to estimate γ as

$$\gamma = \int_0^T p(t)dt.$$

7: To incorporate pulse width modulation, using (5)

$$\hat{x}(t) = \sum_k p\left(\frac{T}{t_{k+1}-t_k}t\right) \otimes \delta(t-t_k).$$

8: Synthesize $\hat{y}(t)$ as follows

$$y_{LF}(t) = \left[\beta+\gamma\right]\left[\alpha + r(t)\right]$$
$$y_{HF}(t) = \left[\alpha + r(t)\right]\left[\hat{x}(t) - \gamma\right]$$
$$\hat{y}(t) = \tau(t) + y_{LF}(t) + y_{HF}(t)$$

where $y[n]$ and $\hat{y}[n]$ are discrete time samples of the signal $y(t)$ and $\hat{y}(t)$, respectively. Also, $\bar{y}$ and $\bar{\hat{y}}$ are the mean of the samples $y[n]$ and $\hat{y}[n]$. A value closer to $\rho = 1$ corresponds to a perfect fit.

The ρ values obtained by fitting the proposed IPFM model to PAP and PVP signals are tabulated in Tables 4, and 5 respectively. For the PAP signals, the ρ between the synthesized and experimental data is, in general, greater than 0.991 except in one case: Pig-4 at PRO-1 and ρ is still greater than 0.980, which indicates an excellent matching between the synthesized signals and their experimental counterparts. For PVP signals, the ρ values are greater than 0.90 except for five stages (three MAC and two PRO). PVP signals with short duration in time have low correlation values.

Figs. 5, and 6 show examples of the experimental and synthesized signals for PAP and PVP signals, respectively, both collected from Pig-2 during MAC-2. The synthesized signals match very well with their experimental counterparts, and this provides a visual verification of the ρ or the correlation results in Tables 4, and 5.

We tried to explore some similar studies to compare the performance with our proposed model. As there do not exist any peripheral

Table 4
Correlation coefficient ρ for the IPFM model in PAP signal.

Subject	MAC-1	MAC-2	MAC-3	PRO-1	PRO-2	PRO-3
Pig-1	0.994	0.992	0.992	0.995	0.995	0.995
Pig-2	0.996	0.997	0.997	0.992	0.995	0.994
Pig-3	0.999	0.999	0.998	0.995	0.992	0.996
Pig-4	0.998	0.997	0.993	0.983	0.996	0.997

Table 5
Orrelation coefficient ρ for the IPFM model in PVP signal.

Subject	MAC-1	MAC-2	MAC-3	PRO-1	PRO-2	PRO-3
Pig-1	0.930	0.927	0.784	0.922	0.912	0.905
Pig-2	0.921	0.904	0.913	0.952	0.954	0.941
Pig-3	0.952	0.959	0.952	0.947	0.957	0.940
Pig-4	0.902	0.884	0.828	0.905	0.871	0.879

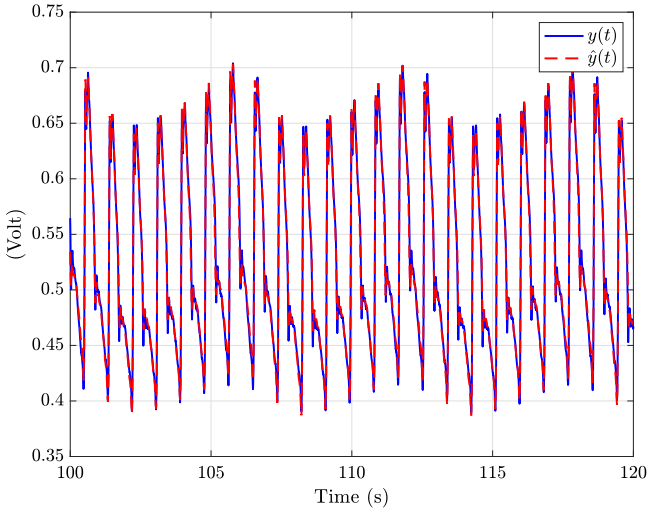

Fig. 5. The PAP signal $y(t)$ and corresponding synthesized signal $\hat{y}(t)$ from Pig-2 MAC-2 with $\rho = 0.997$.

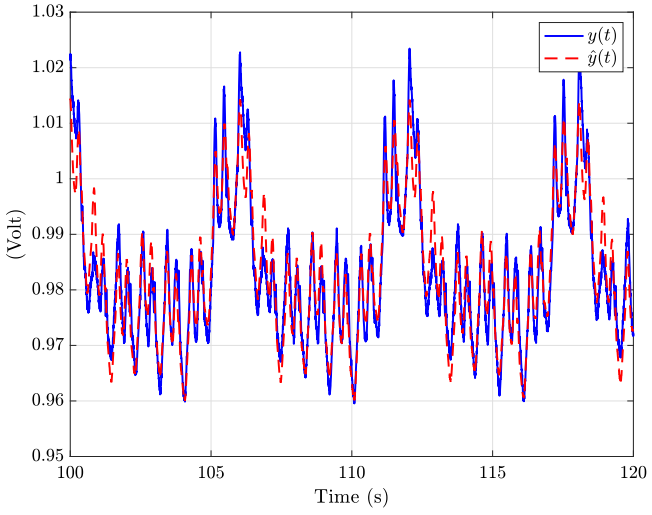

Fig. 6. The PVP signal $y(t)$ and corresponding synthesized signal $\hat{y}(t)$ for Pig-2 MAC-2 with $\rho = 0.904$.

blood pressure signal models to compare with, we tried to compare our results with similar studies on other signals. In [39,40], a model was proposed to reconstruct ECG signals from PPG signals. The reconstruction results are evaluated by using relative root mean-squared error (rRMS) and Pearson's correlation coefficient (ρ). The value of ρ is 0.823

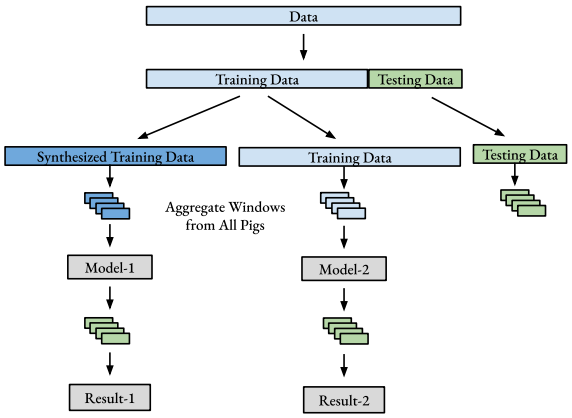

Fig. 7. This diagram explains the training and testing procedures used in Section 5.3. The testing results are reported in Table 6.

and 0.940 on the MIMIC-III dataset under two different segmentation methods used in [40]. In comparison, our average ρ on PAP and PVP signals is 0.995 and 0.914, respectively. We did not use rRMS as a performance metric because it is a biased estimator of performance. Given the contextual nature of model fitting, it is not possible to have a head-to-head comparison with other models. Given the correlation results, our model works well enough when compared to similar models for other signals.

5.3. MAC and PRO classification using logistic regression

In this subsection, the experimental and synthesized pressure signals are used to classify whether a given pig was injected with Isoflurane (different MAC stages), or both Isoflurane and Propofol (different PRO stages). Both are vasodilators but Isoflurane is inhaled and Propofol is injected into the veins. Distinguishing the impacts of these two different vasodilators on the peripheral signals is important. All MAC stages under Isoflurane are combined as a single class. Similarly, all PRO stages under propofol are combined as a second class. The classification is performed by using logistic regression in the frequency domain. For a given pig and for each stage, the total data is split into 70%–30% for training and testing, respectively. These training and testing time domain signals are divided into overlapping 10 s segments or windows. To make the training and testing procedure unbiased, each stage of each pig is divided into equal numbers (70 windows from the training segment and 30 windows from the testing segment) of overlapping time domain windows. Each time domain segment of 10 s is converted to the frequency domain by using the fast Fourier transform (FFT). Frequency domain magnitudes between 0 and 10 Hz are used as the feature vector for logistic regression. Since the window size is 10 s, the frequency domain resolution is 0.1 Hz, thus there are 100 frequency domain samples between 0 and 10 Hz. Finally, the windows are aggregated based on the class. The total number of windows used for MAC and PRO classes during training are $4 \times 3 \times 70 = 840$ each. Similarly, $4 \times 3 \times 30 = 360$ windows are used for each class during testing. Two different classifiers are trained; one uses the experimental data and another one is based on model-synthesized data. The testing is done on experimental testing data for both cases. The whole procedure of classification has been explained in Fig. 7. The classification results are shown in Table 6. In the tables, the results obtained by using the experimental data are shown in parenthesis, and those obtained by using the model-synthesized data are shown outside of the parenthesis.

The classifier based on model-synthesized PAP signals has a better overall accuracy (92.50%) compared to that trained with the experimental data (90.56%), partly due to the fact the modeling process removed some of the noise and artifacts in the experimental data. This

Table 6
MAC and PRO classification results. (The results obtained by using the experimental data are shown in parenthesis, and those obtained by using the model-synthesized data are shown outside of the parenthesis.)

(a) MAC and PRO classification using PAP data.		
–	MAC estimated	PRO estimated
MAC	93.33% (90.56%)	6.67% (9.44%)
PRO	8.33% (9.44%)	91.67% (90.56%)
Accuracy	92.50% (90.56%)	
(b) MAC and PRO classification using PVP data.		
–	MAC estimated	PRO estimated
MAC	85.56% (98.33%)	14.44% (1.67%)
PRO	14.72% (9.44%)	85.28% (90.56%)
Accuracy	85.42% (94.44%)	

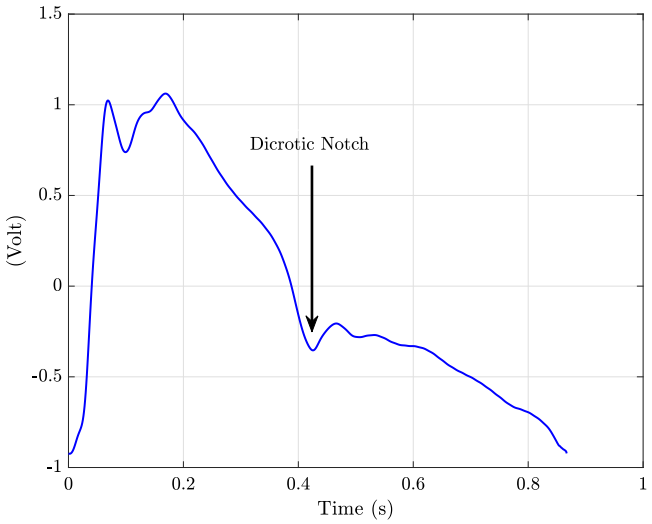

Fig. 8. Dicrotic notch in a PAP pulse $p(t)$ in Pig-2 MAC-2. This notch marks the end of systole and the beginning of diastole.

proves the utility of the model-synthesized signal to retain the valuable information embedded in the signal vital for class discrimination. On the other hand, synthesized PVP signal results have less accuracy (85.42%) compared to the experimental PVP signal results (94.44%). This can be understood from the ρ results presented in Table 5. Here, five stages (three MAC and two PRO) have comparatively bad fitting ($\rho < 0.89$). PVP signals with short duration in time have low correlation values. This relatively bad fitting is probably the reason behind the reduced accuracy in the PVP signal with the model-synthesized data.

5.4. Proposed signal model on CHARIS dataset

The proposed IPFM model is also applied to an open-source blood pressure dataset, the CHARIS dataset [41]. This dataset is part of the larger collection of biomedical signals in the PhysioNet database [42]. CHARIS contains arterial blood pressure recordings from radial arteries of 13 traumatic brain injury human subjects. The signals were sampled at 50 samples/s. Each recording has 1 million samples (5.56 h of recording). The data contain collection anomalies such as abrupt signal level changes and signal discontinuities. In this paper, the IPFM model is fitted to 15-min continuous snippets from each of the recordings, and the correlation coefficient (ρ) is presented in Table 7. The ρ values are consistently above 0.95 for all 13 human subjects. Thus the proposed model is effective in modeling both pig and human ABP signals. Only 15-min signals are used because the proposed IPFM-based model assumes the pulse shape to be stationary. For onset detection, "findpeaks()" function of Matlab has been used as described in 4.3 (see Fig. 9).

Table 7
Correlation coefficient ρ for the IPFM model in CHARIS data with human subjects.

Subject	ρ	Subject	ρ	Subject	ρ
1	0.959	6	0.989	11	0.978
2	0.960	7	0.992	12	0.974
3	0.988	8	0.990	13	0.989
4	0.964	9	0.988	–	–
5	0.983	10	0.990	–	–

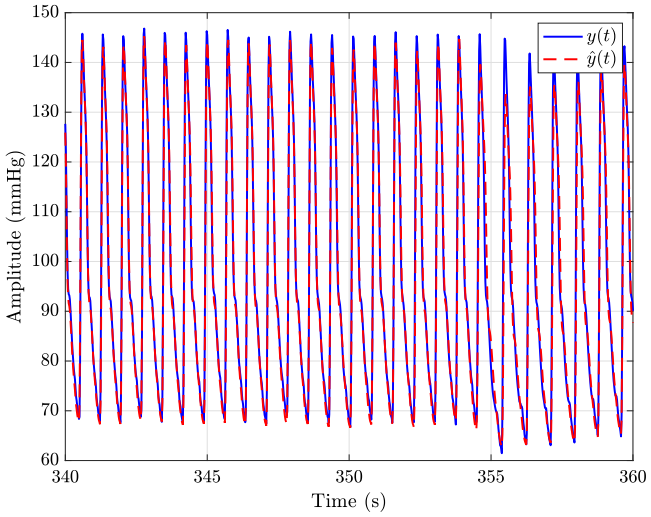

Fig. 9. Comparison of arterial pressure signal $y(t)$ and corresponding model fit $\hat{y}(t)$ from subject 10 of the CHARIS dataset. This 15-min data fit has $\rho = 0.990$.

6. Significance of model parameters

This section discusses the significance of different model parameters under different physiological conditions both qualitatively and quantitatively.

6.1. Unit pulse shapes

For each pulse, the notch after the systolic peak is called the dicrotic notch (Fig. 8). This marks the ending of the systole where the aortic valve closes and the beginning of diastole and ventricular filling. With increasing MAC and PRO levels, the dicrotic notch in $p(t)$ becomes less prominent in the PAP signals (Fig. 10). A similar phenomenon is observed in peripheral arterial and peripheral venous Doppler waveforms [43] and in arterial signals [44]. The dicrotic notch is visible or prominent when the resistance in the arteries and veins is dominant. At a lower resistance, the dicrotic notch is absent and the visual demarcation of systole and diastole is lost. Both Propofol and Isoflurane are vasodilators. Increase in the anesthetic level results in widening of blood vessel and lower vessel impedance. The variations in pulse shape at different anesthesia levels provide the distinguishing features that can be exploited by the classifier. The notch is less visually prominent in PRO signals. It is interesting to note that in PVP signals we do not see any consistent notch and there is no consistent visual distinction in pulses (Fig. 11). This seems quite obvious because the effect of aortic valve closing does not directly impact the PVP signal. There are other factors that contribute to the classification of these signals but pulse shape seems to be a dominant characteristic in PAP signals. It can also be said that under dehydration, the PAP signal shows strong dicrotic notch. On the other hand, the dicrotic notch loses its visual prominence with hydration.

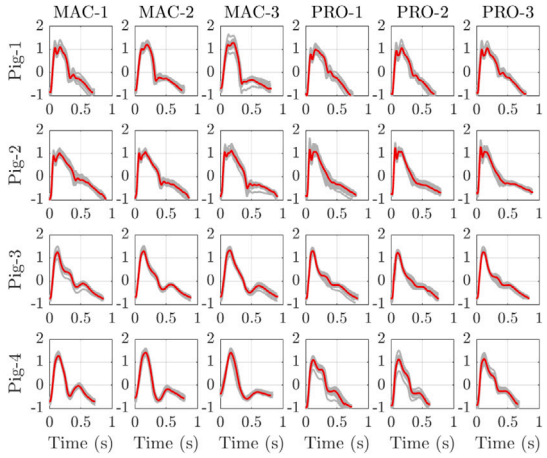

Fig. 10. Pulse shapes in PAP signals at the different anesthetic stages. The red pulses are the aggregate averages of gray pulses and correspond to $\tilde{p}(t)$ of the proposed model, not $p(t)$.

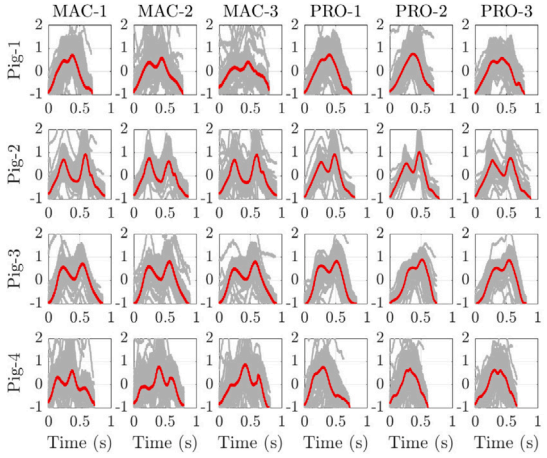

Fig. 11. Pulse shapes in PVP signals at the different anesthetic stages. The red pulses are the aggregate averages of gray pulses and correspond to $\tilde{p}(t)$ of the proposed model, not $p(t)$.

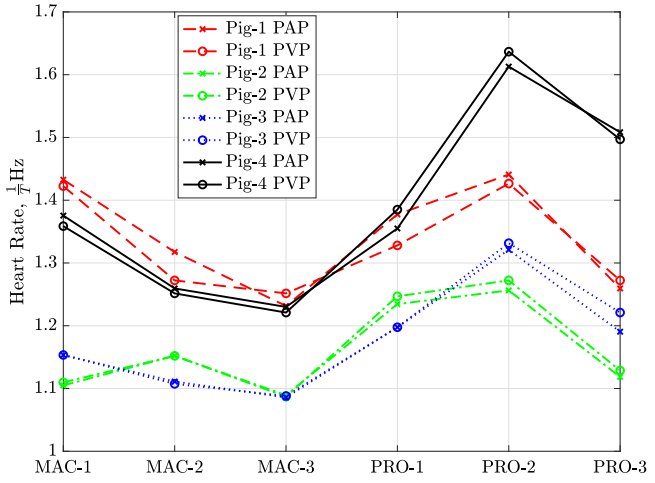

Fig. 12. Change in pulse duration (T) of $\hat{y}(t)$ under different levels of Isoflurane and Propofol based on PAP, and PVP signals.

6.2. Variation in pulse duration

The inverse of the pulse duration (T) is the heart rate ($\frac{1}{T}$). The heart rates of various signals at different anesthesia levels are shown in Fig. 12. The heart rate decreases with the increase of the MAC levels. This is also similar to what happens during dehydration. Under dehydration, the heart beats faster to maintain the cardiac output. With the increase of MAC levels, the heart rate slows down, which is similar to increased hydration. After introducing Propofol, the heart rate initially increases at PRO-1 and PRO-2 but drops at PRO-3. This trend is consistent in all pigs. A similar explanation is not valid for PRO-1 stage, because the trend of heart rate is different here partly due to the fact that before PRO-1 there were other two stages of Isoflurane (2.00% and 1.50%) and the residual effect of these stages (see Table 2). We presume that this is due to the dominant effects of the large doses of vasodilators at this stage. It increases at PRO-2 and decreases at PRO-3, this follows the pattern of heart rate decrease at MAC stages. Initial heart rate increase (at MAC-1 and PRO-1) should be compensatory to vasodilation to maintain cardiac output. The sharp final heart rate drop at PRO-3 is most likely due to the fact that the heart loses its ability to beat spontaneously for higher doses of anesthesia [45].

6.3. Correlation between respiratory and modulating signals

To understand the relationship between the respiratory signal $r(t)$ and the modulating signal $m(t)$, a simple Pearson correlation coefficient has been calculated between $m(t)$ and $r(t)$ for each state that is presented in Fig. 13. These correlation measures can work as indicators of respiratory-induced heart rate variability or respiratory sinus arrhythmia (RSA). A higher correlation between $m(t)$ and $r(t)$ signals indicates that the HRV caused by $m(t)$ is passively influenced by $r(t)$. Based on the results, it can be inferred qualitatively that the negative correlation in the range -0.35 to -0.75 between $m(t)$ and $r(t)$ signal is strong in PAP MAC signals and becomes weaker in PAP PRO signals. This means that the HRV in PAP signal under MAC doses is influenced by the respiratory rate. This is not the case during the PRO stages because by this time the pigs lose their ability to breathe independently and are supported by mechanical ventilation. On the other hand, the correlation is almost nonexistent in PVP signals. Thus it is better to use PAP signals to measure the strength and sources of HRV compared to PVP signals. Based on the data from the four subjects, a stronger correlation between $r(t)$ and $m(t)$ components of the PAP signal can possibly be a good marker or indicator to distinguish MAC and PRO stages. Both being vasodilators, MAC is showing a strong presence of RSA whereas PRO does not.

7. Conclusion

In this paper, we have proposed a new integral pulse frequency modulation-based model for peripheral arterial and venous pressure signals. The model was developed by using arterial and venous pressure data collected from in vivo porcine animal experiments with four female pigs under different levels of anesthesia.

Under proposed model assumption, respiratory signal $r(t)$ is responsible for RSA and modulating signal $m(t)$ is responsible for HRV. The high frequency components of the PVP or PAP signal are both functions of $r(t)$ and $m(t)$. The proposed model isolates these two signals. If the RSA is the sole reason behind HRV then the correlation between $m(t)$ and $r(t)$ should reflect that. To the best of our knowledge, this is the first mathematical model that tries to isolate these two components in the peripheral blood pressure signals.

During dehydration, the blood vessels constrict. On the other hand, vasodilators like Isoflurane and Propofol used in this study broaden the blood vessels. So, increasing doses of vasodilators have similar effect of going from dehydration to hydration. Thus the results obtained in

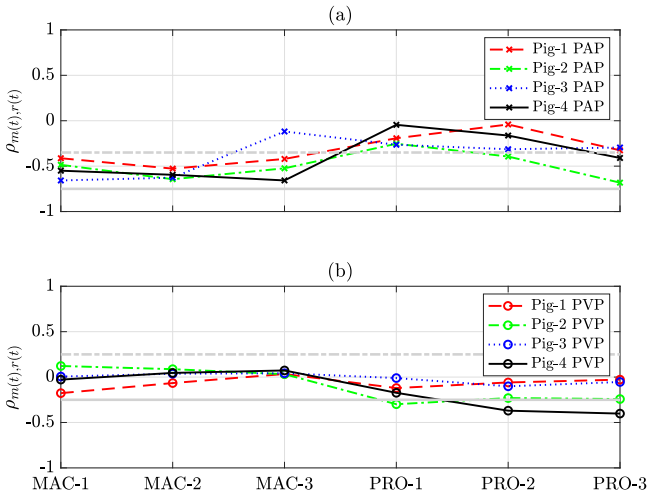

Fig. 13. Correlation coefficients of different states between $m(t)$ and $r(t)$ signals. Panels (a) and (b) are based on PAP and PVP signals respectively. The gray horizontal lines in (a) represent $\rho = -0.35$ and $\rho = -0.75$ respectively. Similarly, in (b) the gray lines represent $\rho = 0.25$ and $\rho = -0.25$ respectively.

this study are applicable to dehydration-like scenario too. This is why vasodilators were used in this study.

The model captures the impacts of multiple physiological factors, such as the heartbeat pulse shape variation, heart rate variation, and correlation between $m(t)$ and $r(t)$. With model parameters estimated from the experimental data, it has been demonstrated that the model-synthesized data match very well with their experimental counterparts, especially for PAP signals. The correlation coefficients of PAP signals are consistently above 0.99 for almost all signals. The correlation coefficient values drop to around 0.90 for PVP signals. Similar results (correlation coefficient > 0.95) have been obtained using the CHARIS dataset of human arterial blood pressure signals. We strongly believe this model can be extended to other similar biomedical signals like PPG, cerebral blood flow velocity, and Doppler waveforms related to cardiac physiology.

The model-synthesized data and experimental data were also used to train a classifier to distinguish between two different types of anesthesia. The proposed model was able to retain meaningful features and achieved comparable classification results with experimental data. The results indicate that both PAP signal and PVP signals can be used to classify different anesthesia levels (and similarly can be used for dehydration). This paper also suggests a possible way to distinguish respiratory-induced heart rate variability from other causes.

For future work, the classification performance can be improved by using information from multiple signals collected from peripheral regions in a minimally invasive way, instead of just using one signal. In addition, we would like to further improve the model by addressing some of its current limitations. Some limitations of the current model include: (1) The pulse shape is assumed stationary across the entire signal duration. A more effective approach would be to divide the signal into segments and consider stationary pulse shapes in each smaller time segment. (2) The assumption of $e_u(t) = -e_l(t)$ was used in the model development. This assumption is not always valid. A more general approach would be to assume $e_u(t) = \phi e_l(t)$, where $\phi \in \mathbb{R}$. A more efficient upper and lower envelope detection algorithm can help to further improve the estimation accuracy of the modulating signal $m(t)$. (3) A better pulse onset detection method can be used for PVP signals. (4) Although time was allotted for inhalation concentration to fall to sub-therapeutic levels when transitioning from Isoflurane to Propofol, the experimental setup lacked the equipment to confirm the end-tidal concentration of Isoflurane was at or near zero. Residual inhalation anesthesia (Isoflurane) could be contributing to initial Propofol measurements. Ideally resourced, future work would examine intravenous agents independently from the moment of induction.

All supplementary materials and codes of this paper can be found at this Github repository: https://github.com/i2pt/MPAVPSwIPFM.

CRediT authorship contribution statement

Md Abul Hayat: Methodology, Software, Validation, Formal analysis, Writing – original draft, Writing – review & editing, Visualization. **Jingxian Wu:** Methodology, Formal analysis, Writing – original draft, Writing – review & editing, Supervision, Funding acquisition. **Sam Stephens:** Conceptualization, Investigation, Data curation. **Hanna K. Jensen:** Conceptualization, Investigation, Writing – original draft. **Adrià A. Villafranca:** Conceptualization, Investigation, Data curation. **Joseph A. Sanford:** Conceptualization, Investigation, Resources, Writing – original draft. **Kevin W. Sexton:** Conceptualization, Investigation, Resources, Writing – original draft, Funding acquisition. **Morten O. Jensen:** Conceptualization, Investigation, Resources, Writing – original draft, Supervision.

Declaration of competing interest

The authors declare that they have no known competing financial interests or personal relationships that could have appeared to influence the work reported in this paper.

Data availability

The data that has been used is confidential.

Acknowledgments

Research reported in this publication was supported by the National Center for Advancing Translational Sciences of the National Institutes of Health, USA under award numbers UL1 TR003107 and TL1 TR003109. The content is solely the responsibility of the authors and does not necessarily represent the official views of the National Institutes of Health. It was also supported in part by the U.S. National Science Foundation (NSF) under Award Number ECCS-1711087 and the Arkansas Research Alliance.

Appendix A. Derivation of Eq. (8)

From (3), $\theta(t_k) = kT - t_k$ and $\theta'(t_k) = m(t_k)$. Using the properties of delta function [46], if a function $g(t)$ has only one root at $t = t_k$, then

$$\delta[g(t)] = \frac{1}{|g'(t_k)|}\delta(t - t_k) = \frac{1}{|g'(t)|}\delta(t - t_k),$$

or

$$\delta[g(t)] \cdot |g'(t_k)| = \delta[g(t)] \cdot |g'(t)| = \delta(t - t_k).$$

Assuming $g(t) = t - kT + \theta(t)$ yields $g'(t) = 1 + m(t)$. Replacing $g(t)$ and $g'(t)$ in (7) gives

$$s(t) = \sum_k \delta(t - t_k),$$
$$= |1 + m(t)| \sum_k \delta\big[t - kT + \theta(t)\big].$$

Using Fourier series

$$\sum_{k=-\infty}^{\infty} \delta(t - kT) = \frac{1}{T}\sum_{n=-\infty}^{\infty} e^{jn\frac{2\pi}{T}t},$$

$$\sum_{k=-\infty}^{\infty} \delta\big[t - kT + \theta(t)\big] = \frac{1}{T}\sum_{n=-\infty}^{\infty} e^{jn\frac{2\pi}{T}\left[t+\theta(t)\right]}$$

Using the relation above,

$$s(t) = \frac{|1+m(t)|}{T} \sum_{n=-\infty}^{\infty} e^{jn\frac{2\pi}{T}\left[t+\theta(t)\right]}$$
$$= \frac{|1+m(t)|}{T} \left\{ 1 + 2\sum_{n=1}^{\infty} \cos\left[n\frac{2\pi}{T}\left(t+\theta(t)\right)\right] \right\}$$
$$= \frac{1+m(t)}{T} \left\{ 1 + 2\sum_{n=1}^{\infty} \cos\left[n\frac{2\pi}{T}\left(t+\theta(t)\right)\right] \right\}$$

where the last equality follows from the fact that $|1+m(t)| = 1+m(t)$ as $|m(t)| \ll 1$. This proof assumes $k \in \mathbb{Z}$. Whereas in the rest of the paper assumes $k \in \mathbb{Z}^+$. The only reason to assume $k \in \mathbb{Z}^+$ is for practical numerical convenience without loss of generality.

References

[1] S. Kim, S. Park, J. Cui, J. Lee, S. Cho, W. Chae, H. Jin, K. Hwang, Peripheral venous pressure as an alternative to central venous pressure in patients undergoing laparoscopic colorectal surgery, Br. J. Anaesth. 106 (3) (2011) 305–311.

[2] D. De Backer, J.-L. Vincent, Should we measure the central venous pressure to guide fluid management? Ten answers to 10 questions, Crit. Care 22 (1) (2018) 43.

[3] A. Anter, R. Bondok, Peripheral venous pressure is an alternative to central venous pressure in paediatric surgery patients, Acta Anaesthesiol. Scand. 48 (9) (2004) 1101–1104.

[4] J.R. Munis, S. Bhatia, L.J. Lozada, Peripheral venous pressure as a hemodynamic variable in neurosurgical patients, Anesth. Analg. 92 (1) (2001) 172–179.

[5] B.W. Sperry, J. Campbell, M. Yanavitski, S. Kapadia, W.W. Tang, M. Hanna, Peripheral venous pressure measurements in patients with acute decompensated heart failure (PVP-HF), Circulation: Heart Fail. 10 (7) (2017) e004130.

[6] B. Sileshi, K.M. Hocking, R.B. Boyer, F.J. Baudenbacher, K.L. Kohurst, C.M. Brophy, S. Eagle, Peripheral venous waveform analysis for detecting early hemorrhage: a pilot study, Intensive Care Med. 41 (6) (2015) 1147–1148.

[7] P.C. Bonasso, M.S. Dassinger, M.O. Jensen, S.D. Smith, J.M. Burford, K.W. Sexton, Optimizing peripheral venous pressure waveforms in an awake pediatric patient by decreasing signal interference, J. Clin. Monit. Comput. 32 (6) (2018) 1149–1153.

[8] P.C. Bonasso, K.W. Sexton, A. Hayat, A. Al-Alawi, J. Wu, H.K. Jensen, M.O. Jensen, S.D. Smith, J.M. Burford, M.S. Dassinger III, Venous physiology predicts anesthetic induced hypotension in infants, J. Am. Coll. Surg. 227 (4) (2018) e116.

[9] P.C. Bonasso, K.W. Sexton, S.C. Mehl, M.S. Golinko, M.A. Hayat, J. Wu, M.O. Jensen, S.D. Smith, J.M. Burford, M.S. Dassinger, Lessons learned measuring peripheral venous pressure waveforms in an anesthetized pediatric population, Biomed. Phys. Eng. Express 5 (3) (2019) 035020.

[10] M.A. Hayat, J. Wu, P.C. Bonasso, K.W. Sexton, H.K. Jensen, M.S. Dassinger, M.O. Jensen, Unsupervised anomaly detection in peripheral venous pressure signals with hidden Markov models, Biomed. Signal Process. Control 62 (2020) 102126.

[11] L.D. Crimmins-Pierce, G.P. Bonvillain, K.R. Henry, M.A. Hayat, A.A. Villafranca, S.E. Stephens, H.K. Jensen, J.A. Sanford, J. Wu, K.W. Sexton, et al., Critical information from high fidelity arterial and venous pressure waveforms during anesthesia and hemorrhage, Cardiovasc. Eng. Technol. (2022) 1–13.

[12] A.Z. Al-Alawi, K.R. Henry, L.D. Crimmins, P.C. Bonasso, M.A. Hayat, M.S. Dassinger, J.M. Burford, H.K. Jensen, J. Sanford, J. Wu, et al., Anesthetics affect peripheral venous pressure waveforms and the cross-talk with arterial pressure, J. Clin. Monit. Comput. 36 (1) (2022) 147–159.

[13] P.C. Bonasso, K.W. Sexton, M.A. Hayat, J. Wu, H.K. Jensen, M.O. Jensen, J.M. Burford, M.S. Dassinger, Venous physiology predicts dehydration in the pediatric population, J. Surg. Res. 238 (2019) 232–239.

[14] A. Alalawi, Using Peripheral Venous Pressure Waveforms to Predict Key Hemodynamic Parameters, University of Arkansas, 2019.

[15] A.Z. Al-Alawi, K.R. Henry, L.D. Crimmins, P.C. Bonasso, M.A. Hayat, M.S. Dassinger, J.M. Burford, H.K. Jensen, J. Sanford, J. Wu, et al., Anesthetics affect peripheral venous pressure waveforms and the cross-talk with arterial pressure, J. Clin. Monit. Comput. (2021) 1–13.

[16] L. Nilsson, A. Johansson, S. Kalman, Respiratory variations in the reflection mode photoplethysmographic signal. Relationships to peripheral venous pressure, Med. Biol. Eng. Comput. 41 (3) (2003) 249–254.

[17] D. Martin-Martinez, P. Casaseca-de-la-Higuera, M. Martin-Fernandez, C. Alberola-López, Stochastic modeling of the PPG signal: a synthesis-by-analysis approach with applications, IEEE Trans. Biomed. Eng. 60 (9) (2013) 2432–2441.

[18] Q. Tang, Z. Chen, J. Allen, A. Alian, C. Menon, R. Ward, M. Elgendi, PPGSynth: An innovative toolbox for synthesizing regular and irregular photoplethysmography waveforms, Front. Med. (2020) 735.

[19] Q. Tang, Z. Chen, R. Ward, M. Elgendi, Synthetic photoplethysmogram generation using two Gaussian functions, Sci. Rep. 10 (1) (2020) 1–10.

[20] M. Chen, Q. Zhu, M. Wu, Q. Wang, Modulation model of the photoplethysmography signal for vital sign extraction, IEEE J. Biomed. Health Inf. 25 (4) (2020) 969–977.

[21] N. Jafarnia-Dabanloo, D. McLernon, H. Zhang, A. Ayatollahi, V. Johari-Majd, A modified zeeman model for producing HRV signals and its application to ECG signal generation, J. Theoret. Biol. 244 (2) (2007) 180–189.

[22] M. Boulakia, S. Cazeau, M.A. Fernández, J.-F. Gerbeau, N. Zemzemi, Mathematical modeling of electrocardiograms: a numerical study, Ann. Biomed. Eng. 38 (3) (2010) 1071–1097.

[23] M. Quiroz-Juárez, O. Jiménez-Ramírez, R. Vázquez-Medina, V. Breña-Medina, J. Aragón, R. Barrio, Generation of ECG signals from a reaction-diffusion model spatially discretized, Sci. Rep. 9 (1) (2019) 1–10.

[24] M.A. Awal, S.S. Mostafa, M. Ahmad, M.A. Alahe, M.A. Rashid, A.Z. Kouzani, M.P. Mahmud, Design and optimization of ECG modeling for generating different cardiac dysrhythmias, Sensors 21 (5) (2021) 1638.

[25] E.J. Bayly, Spectral analysis of pulse frequency modulation in the nervous systems, IEEE Trans. Biomed. Eng. (4) (1968) 257–265.

[26] O. Rompelman, J.B. Snijders, C.J. Van Spronsen, The measurement of heart rate variability spectra with the help of a personal computer, IEEE Trans. Biomed. Eng. (7) (1982) 503–510.

[27] J. Mateo, P. Laguna, New heart rate variability time-domain signal construction from the beat occurrence time and the IPFM model, in: Computers in Cardiology 1996, IEEE, 1996, pp. 185–188.

[28] J. Mateo, P. Laguna, Improved heart rate variability signal analysis from the beat occurrence times according to the IPFM model, IEEE Trans. Biomed. Eng. 47 (8) (2000) 985–996.

[29] J. Mateo, P. Laguna, Analysis of heart rate variability in the presence of ectopic beats using the heart timing signal, IEEE Trans. Biomed. Eng. 50 (3) (2003) 334–343.

[30] R. Bailón, P. Laguna, L. Mainardi, L. Sornmo, Analysis of heart rate variability using time-varying frequency bands based on respiratory frequency, in: 2007 29th Annual International Conference of the IEEE Engineering in Medicine and Biology Society, IEEE, 2007, pp. 6674–6677.

[31] J. Lázaro, E. Gil, J.M. Vergara, P. Laguna, Pulse rate variability analysis for discrimination of sleep-apnea-related decreases in the amplitude fluctuations of pulse photoplethysmographic signal in children, IEEE J. Biomed. Health Inf. 18 (1) (2013) 240–246.

[32] ADInstruments, Pressure catheters, 2023, Accessed: 2023-03-20 URL: https://www.adinstruments.com/products/pressure-catheters.

[33] P. Laguna, L. Sörnmo, Modelling heart rate variability, in: Proceedings of the Sixteenth International Symposium on Mathematical Theory of Networks and Systems, Loeven, 2004, pp. 1–6.

[34] M. Brennan, M. Palaniswami, P. Kamen, Do existing measures of poincare plot geometry reflect nonlinear features of heart rate variability? IEEE Trans. Biomed. Eng. 48 (11) (2001) 1342–1347.

[35] M.S. Manikandan, K. Soman, A novel method for detecting R-peaks in electrocardiogram (ECG) signal, Biomed. Signal Process. Control 7 (2) (2012) 118–128.

[36] H.S. Shin, C. Lee, M. Lee, Adaptive threshold method for the peak detection of photoplethysmographic waveform, Comput. Biol. Med. 39 (12) (2009) 1145–1152.

[37] S. Asgari, N. Canac, R. Hamilton, F. Scalzo, Identification of pulse onset on cerebral blood flow velocity waveforms: A comparative study, BioMed Res. Int. 2019 (2019).

[38] W. Zong, T. Heldt, G. Moody, R. Mark, An open-source algorithm to detect onset of arterial blood pressure pulses, in: Computers in Cardiology, 2003, IEEE, 2003, pp. 259–262.

[39] Q. Zhu, X. Tian, C.-W. Wong, M. Wu, ECG reconstruction via PPG: A pilot study, in: 2019 IEEE EMBS International Conference on Biomedical & Health Informatics, BHI, IEEE, 2019, pp. 1–4.

[40] Q. Zhu, X. Tian, C.-W. Wong, M. Wu, Learning your heart actions from pulse: ECG waveform reconstruction from PPG, IEEE Internet Things J. 8 (23) (2021) 16734–16748.

[41] N. Kim, A. Krasner, C. Kosinski, M. Wininger, M. Qadri, Z. Kappus, S. Danish, W. Craelius, Trending autoregulatory indices during treatment for traumatic brain injury, J. Clin. Monit. Comput. 30 (6) (2016) 821–831.

[42] A.L. Goldberger, L.A. Amaral, L. Glass, J.M. Hausdorff, P.C. Ivanov, R.G. Mark, J.E. Mietus, G.B. Moody, C.-K. Peng, H.E. Stanley, PhysioBank, PhysioToolkit, and PhysioNet: components of a new research resource for complex physiologic signals, Circulation 101 (23) (2000) e215–e220.

[43] E.S. Kim, A.M. Sharma, R. Scissons, D. Dawson, R.T. Eberhardt, M. Gerhard-Herman, J.P. Hughes, S. Knight, A. Marie Kupinski, G. Mahe, et al., Interpretation of peripheral arterial and venous Doppler waveforms: A consensus statement from the society for vascular medicine and society for vascular ultrasound, Vasc. Med. 25 (5) (2020) 484–506.

[44] M. Nirmalan, P.M. Dark, Broader applications of arterial pressure wave form analysis, Contin. Educ. Anaesth. Crit. Care Pain 14 (6) (2014) 285–290.

[45] S. Eis, J. Kramer, Anesthesia inhalation agents cardiovascular effects, in: StatPearls [Internet], StatPearls Publishing, 2021, pp. 1–8.

[46] E.W. Weisstein, Delta function, 2023, Accessed: 2023-03-20 https://mathworld.wolfram.com/DeltaFunction.html.